ACS MATERIALS LETTERS

www.acsmaterialsletters.org

LETTER

Cancer Cell-Specific Autophagy Activation Using Phosphorus-Based Nanoplatform as Anabolism Activator

Yiqi Li,[‡] Qilong Fang,[‡] Jiang-Yi-Hui Sheng,[‡] Xiaodong Hu,[‡] Yanbing Yang, Yun Zhang, Long Chen, Jie Tan,* Quan Yuan,* and Weihong Tan

Cite This: *ACS Materials Lett.* 2023, 5, 2028–2038

Read Online

ACCESS | Metrics & More | Article Recommendations | Supporting Information

ABSTRACT: Autophagy suppresses tumorigenesis by restoring a favorable energy balance. Activation of autophagic pathways has therefore sparked great interest as a target for cancer therapy. However, the targets of available autophagy activators are nonexclusively involved in autophagy in cancer cells, thus causing cytotoxicity in noncancerous tissues. Stimulation of anabolism and ensuing decreased energy levels in cancer cells are central to tumor-selective autophagy induction. Herein, we present black phosphorus quantum dots (BPQDs) with red blood cell membranes (RBCMs) cloaking (BPQDs@RBCMs) as activators of tumor anabolism for tumor-specific autophagy activation. The selective degradation of BPQDs@RBCMs releasing phosphate in the tumor microenvironment initiates autophagy by falling energy levels. *In vivo* assessments confirm that the BPQDs@RBCMs treatment effectively reduces overall tumor burden and alters metabolite profiles in tumor. Overall, this study underlines the potential utility of tumor-selective autophagy induction in cancer therapeutics.

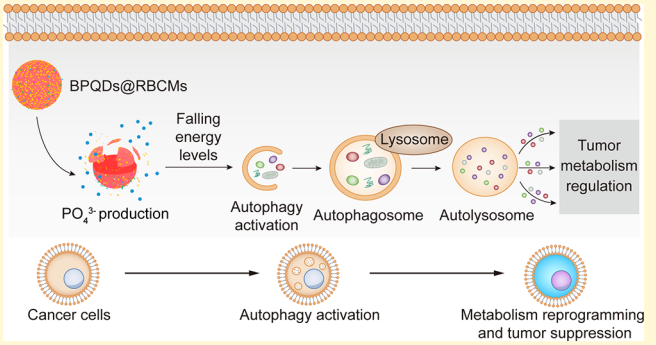

Cells have evolved a sophisticated system that maintains the balance between catabolism and anabolism to meet their energy and nutrient needs.[1,2] Autophagy is an adaptive process in response to low-energy conditions and cell stresses.[1,3,4] Once initiated, autophagy acts to restore energy balance by eliminating damaged proteins and organelles and by promoting ATP production.[5,6] Metabolic regulation by autophagy is thought to have a key role in the suppression of tumorigenesis.[7−10] By reducing ROS and genome damage, maintaining cellular homeostasis and improving stress response, autophagy effectively inhibits malignant transformation and serves as a tumor-suppressive mechanism.[6,7,10] Hence, activating autophagy in cancer cells will present opportunities for the cancer therapeutics by regulation of tumor metabolism.[8,11]

Autophagy as a target in cancer therapy has motivated the preclinical and clinical development of autophagy activators, including rapamycin and metformin.[8,12] However, several components of the autophagic pathways operate in multiple cellular processes at the whole-body level.[11,13] Currently available autophagy activators usually have limited specificity for the autophagic pathways, thus causing cytotoxicity in noncancerous tissues and mediating autophagy-independent functions.[3,8,11,12] For example, rapamycin not only activates autophagy but also has robust immunosuppressive effects and inhibits cellular growth and proliferation.[11] Therefore, approaches that target cancer cell-specific autophagy activation need to be explored to circumvent these adverse effects.[8,12] The key to tumor-selective autophagy comes from the falling energy status in cancer cells.[1,6,14] Once the energy levels in cancer cells fall, AMP-activated protein kinase (AMPK), the cellular energy sensor initiates autophagy in cancer cells to conserve energy, whereas the autophagy in normal cells is unaffected.[1,14] When the anabolic pathways are switched on, the biosynthesis of lipids and proteins will accelerate, leading to bioenergetic crisis due to rapid ATP consumption together with ADP and AMP generation.[15,16] Then, AMPK senses the increases in AMP/ATP and ADP/ATP ratios, thereby

Received: March 13, 2023
Accepted: June 26, 2023
Published: June 29, 2023

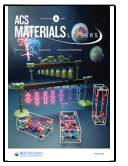

https://doi.org/10.1021/acsmaterialslett.3c00256
ACS Materials Lett. 2023, 5, 2028–2038

Scheme 1. Schematic Illustration Showing Tumor-Selective Autophagy Activation by BPQDs@RBCMs-Promoted Anabolism[a]

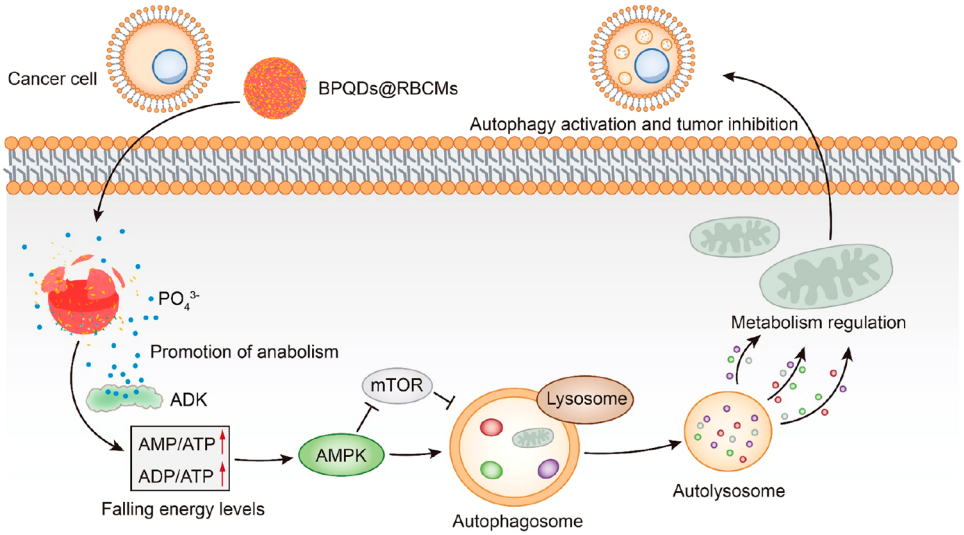

[a]The BPQDs@RBCMs are selectively degraded in cancer cells and produce phosphate, thereby enhancing adenosine kinase (ADK) activity and promoting anabolism. The increased anabolism switches on AMPK pathways, then induces tumor-selective autophagy and regulates tumor metabolism to inhibit tumor growth.

triggering autophagy.[14,17,18] Thus, promoting anabolism and decreasing the energy levels in cancer cells represent desirable strategies for tumor-selective autophagy activation.[19,20]

Addition of extra phosphate that responses to tumor microenvironment will perform a crucial role in stimulating anabolism in cancer cells but has a minor role in normal cells,[21−23] hence selectively targeting autophagy activation in tumor. Herein, we present black phosphorus quantum dots (BPQDs) with red blood cell membranes (RBCMs) cloaking (BPQDs@RBCMs) as activators of tumor anabolism for tumor-selective autophagy activation (Scheme 1). BPQDs, the biocompatible crystals consisting of only phosphorus atoms, exhibit fast intracellular biodegradation in tumor microenvironment due to the strong intracellular oxidative stress and acidic conditions, generating phosphate as the major product.[23] The degradation of BPQDs releasing phosphate in the tumor microenvironment promotes the tumor anabolism. RBCMs are natural long-circulating delivery carriers, where their membrane proteins play a vital role on immune-evasive functions.[24,25] The merits of RBCMs as carriers to load BPQDs include evading the immune system and extending the blood circulation half-life. The results suggest that BPQDs@RBCMs degradation gives rise to a faster elevation of AMP/ATP and ADP/ATP ratios and lower energy levels in cancer cells than in normal cells. *In vitro* experiments have demonstrated that BPQDs@RBCMs treatment leads to the AMPK phosphorylation, the inhibition of mammalian target of rapamycin (mTOR) activity, the conversion of microtubule-associated light chain 3 (LC3)-I to LC3-II, and formation of autophagic structures. *In vivo* assessments further confirm the suppression of bladder cancer development by BPQDs@RBCMs and their contributions to significant metabolic changes. Collectively, we show that BPQDs@RBCMs can selectively trigger tumor autophagy by increasing anabolism, thereby inhibiting tumor growth and reprogramming metabolism.

The BPQDs were fused with processed RBCMs to fabricate BPQDs@RBCMs (Figure 1a). To begin, BPQDs were prepared using a liquid exfoliation method (Figure S1). Figure 1b shows the typical transmission electron microscope (TEM) images of well-dispersed uniform BPQDs, with an average lateral size of 3 nm (Figure 1c). Next, purified mouse RBCMs from whole blood were extruded through porous membranes to generate BPQDs@RBCMs. The TEM images show that BPQDs@RBCMs were deformed into spherical shapes and were approximately 150 nm in size (Figures 1d, S2, and S3). To further confirm the successful fusion of RBCMs with BPQDs, the zeta potentials of BPQDs, RBCMs, and BPQDs@RBCMs were measured. As shown in Figure 1e, the surface zeta potential of BPQDs changed from −20 to −10 mV upon fusing with RBCMs, similar to the zeta potential of RBCMs (−9 mV), indicating the successful fusion. By measuring the amount of BPQDs in the supernatant, we found that BPQDs@RBCMs have an encapsulation efficiency of 70% (Figure S4). The membrane proteins of RBCMs could help BPQDs escape the immune system. To confirm that BPQDs@RBCMs maintain the protein composition of RBCMs, membrane proteins on the surface of BPQDs@RBCMs were examined by sodium dodecyl sulfate polyacrylamide gel electrophoresis (SDS-PAGE). As presented in Figure 1f, three protein brands for BPQDs@RBCMs, red blood cells (RBCs) and RBCMs displayed the same stripes, indicating that the membrane proteins were reserved during the extrusion. All the above results demonstrated the successful preparation of BPQDs@RBCMs.

Owing to the acidity and strong intracellular oxidative stress in tumor microenvironment, BPQDs@RBCMs may degrade faster in cancer cells, leading to selective elevation of phosphate anions and promotion of anabolism in cancer cells.[23,26,27] To assess the degradation of BPQDs@RBCMs and resultant phosphate production, we studied the stability of BPQDs@RBCMs in simulated normal physiological environment and acidic tumor microenvironment with strong oxidative stress by phosphate assay kit, ultraviolet (UV)-visible spectrophotometer, and confocal Raman microscope (Figure 1g). Fast elevation of the dissolved phosphate concentration and decrease in the absorbance intensity at 410 nm were observed, indicating the degradation of BPQDs@RBCMs in both

https://doi.org/10.1021/acsmaterialslett.3c00256
ACS Materials Lett. 2023, 5, 2028−2038

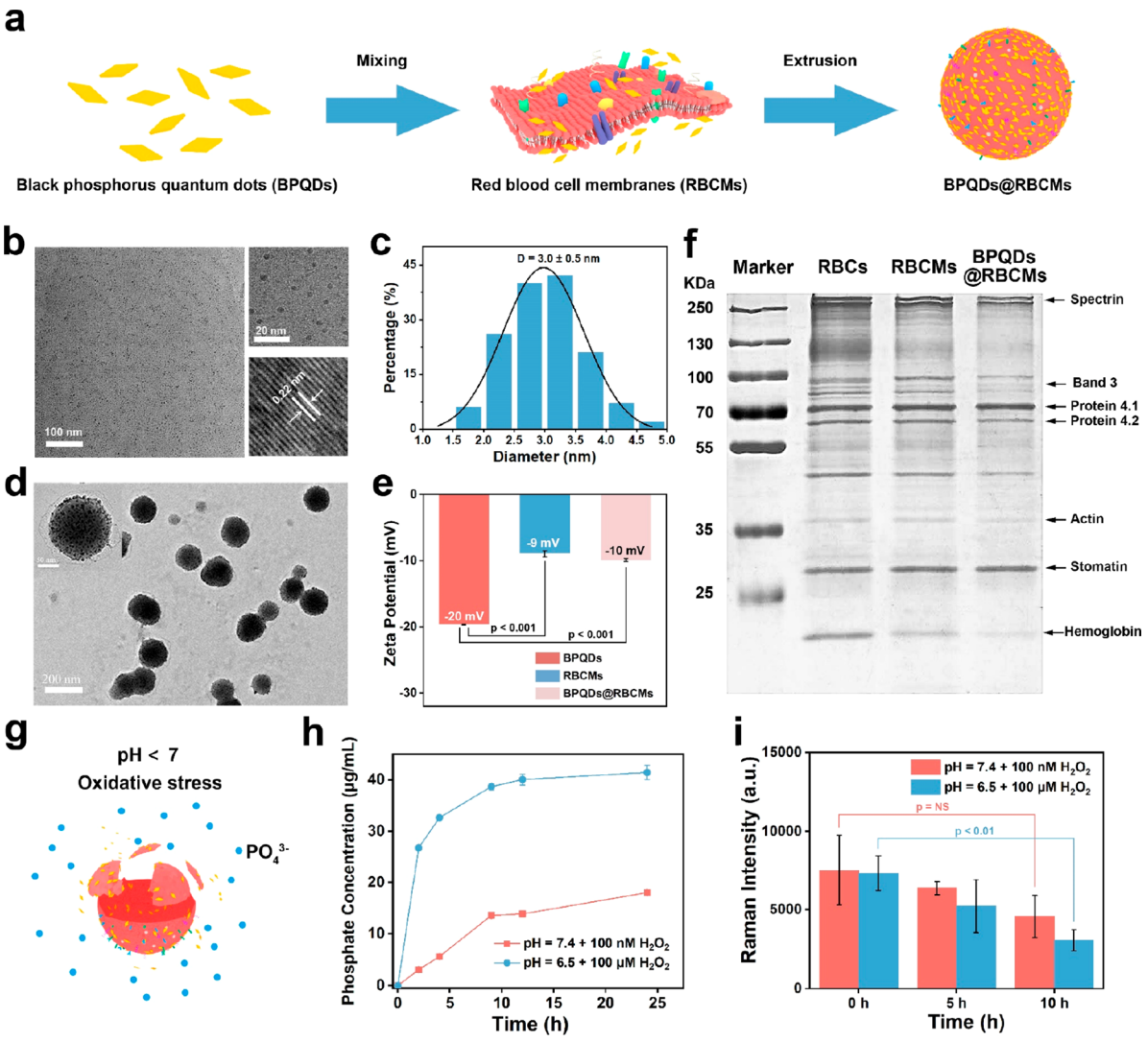

Figure 1. Preparation and characterization of BPQDs@RBCMs. (a) Schematic illustration of the preparation of BPQDs@RBCMs, including the hemolysis to acquire RBCMs and the extrusion to prepare BPQDs@RBCMs. (b) TEM (left and top right) and high-resolution transmission electron microscopy (HRTEM) (bottom right) images of BPQDs. The HRTEM image shows that the lattice spacing of BPQDs is about 0.2 nm. (c) Size distribution of BPQDs obtained from the TEM images. (d) TEM images of BPQDs@RBCMs, indicating that the BPQDs were uniformly attached to the RBCMs. The inset displays BPQDs@RBCMs with magnification (scale bar, 50 nm). (e) Surface zeta potential of BPQDs, RBCMs, and BPQDs@RBCMs. Data are means ± SD (n = 3). (f) Proteins in empty RBCs, RBCMs, and BPQDs@RBCMs resolved on a polyacrylamide gel. The arrows indicate the protein composition of RBCMs. Marker: protein marker. (g) Schematic diagram of BPQDs@RBCMs degradation and resultant phosphate production in tumor microenvironment. (h) Concentration of phosphate produced by BPQDs@RBCMs versus time in different simulated environments. Solution containing 100 nM H_2O_2 and with a pH value of 7.4 was used to mimic the normal physiological environment. Another solution (pH 6.5, 100 μM H_2O_2) was used to simulate the tumor microenvironment. Data are means ± SD (n = 3). (i) Average Raman intensity of BPQDs versus time in different simulated environments. The average Raman signal intensity was calculated by determining the total area of the three characteristic Raman peaks (A_g^1, B_{2g}, and A_g^2). Data are means ± SD (n = 3). NS: Not significant.

environments (Figures 1h and S5). After 24 h, the absorbance of the BPQDs@RBCMs at 410 nm decreased by 95% and phosphate production reached 40 μg/mL in simulated tumor microenvironment, suggesting that BPQDs@RBCMs were degraded more rapidly in simulated tumor microenvironment. The total area of three characteristic Raman peaks of BPQDs can also be employed to investigate the degradation of BPQDs@RBCMs.[23,26] The relative amount of BPQDs@RBCMs at different time points in two simulated environments was further determined by monitoring the Raman intensity mapping and by average intensities of the three characteristic Raman peaks of BPQDs. With ongoing time, the degradation becomes more evident in simulated tumor microenvironment, where the BPQDs@RBCMs lose approximately 60% of total intensity after 10 h, whereas the BPQDs@RBCMs in simulated normal environment degraded by less than 40% (Figure 1i). The above results demonstrate that BPQDs@RBCMs were degraded rapidly in simulated tumor microenvironment and could give rise to selective elevation of intracellular phosphate concentration and promotion of anabolism in cancer cells.

Adenosine kinase (ADK) catalyzes the phosphorylation of adenosine (Ado) to AMP according to the reaction: Ado + ATP → AMP + ADP.[28,29] Thus, ADK activation increases anabolism by consuming ATP while producing AMP and ADP.[21,30,31] ADK activity is strongly dependent on phosphate concentration, where phosphate facilitates the binding of Ado

https://doi.org/10.1021/acsmaterialslett.3c00256
ACS Materials Lett. 2023, 5, 2028−2038

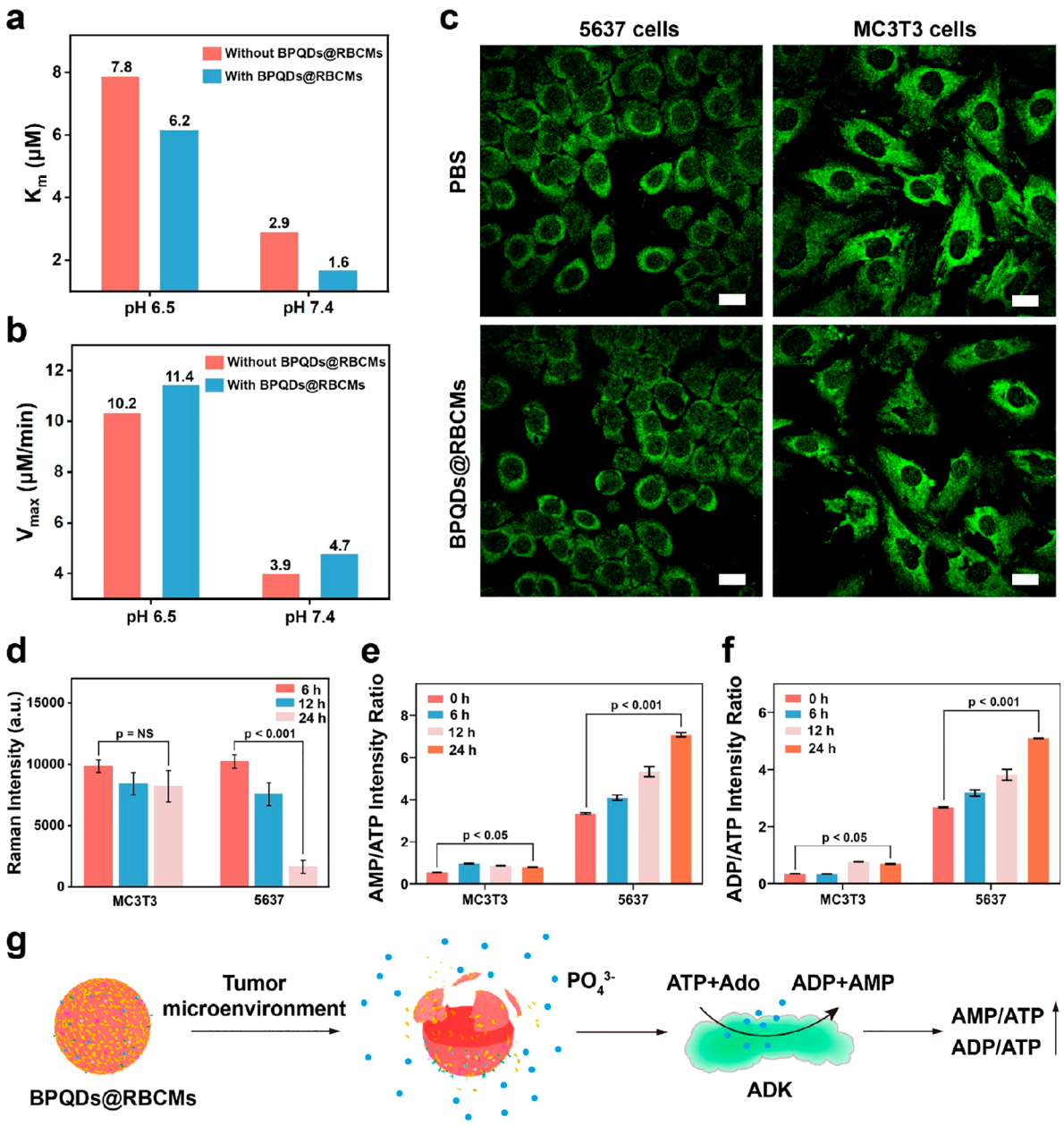

Figure 2. Selective degradation of BPQDs@RBCMs leads to promotion of anabolism. (a, b) The effect of BPQDs@RBCMs on ADK-catalyzed reaction at pH 6.5 and pH 7.4. The K_m (a) and V_{max} (b) for the reaction catalyzed by ADK in pH 6.5 and 7.4 solutions were calculated according to the AMP production with or without BPQDs@RBCMs treatment. (c) Immunofluorescenc of ADK using the ADK antibody in 5637 cancer cells and MC3T3 normal cells treated with BPQDs@RBCMs or phosphate buffered saline (PBS). Scale bar: 20 μm. (d) The degradation of BPQDs@RBCMs in MC3T3 and 5637 cells at different time points monitored by Raman scattering. The average Raman signal intensity was calculated by determining the total area of the three characteristic Raman peaks (A_g^1, B_{2g}, and A_g^2). Data are means ± SD (n = 3). NS: Not significant. (e) AMP/ATP ratios in MC3T3 and 5637 cells with BPQDs@RBCMs treatment for different time. Data are means ± SD (n = 3). (f) ADP/ATP ratios in MC3T3 and 5637 cells treated with BPQDs@RBCMs for different time. Data are means ± SD (n = 3). (g) Schematic diagram showing the selective degradation of BPQDs@RBCMs in response to the tumor microenvironment and the resultant ADK activity enhancement. Finally, the intracellular AMP/ATP and ADP/ATP ratios increase dramatically as a result of the ADK-catalyzed reaction, which signifies the falling cellular energy levels.

near the catalytic residue and forms an intermediate with ATP.[32,33] Therefore, the elevated phosphate concentration brings about the dramatic enhancement of ADK activity, leading to increased anabolism and falling energy levels.[34,35] Next, we examined the effect of BPQDs@RBCMs degradation on ADK catalytic activity to promote anabolism. BPQDs@RBCMs were dispersed in buffer solutions with pH values of 7.4 and 6.5, and the ADK activity was tested after the complete degradation of BPQDs@RBCMs in two solutions. In both environments, the addition and degradation of BPQDs@RBCMs caused a significant increase in AMP generation (Figure S6). In comparison with the group without BPQDs@RBCMs, the lower Michaelis constant (K_m) and higher maximal reaction velocity (V_{max}) had been observed for ADK in the BPQDs@RBCMs group (Figure 2a and 2b). These results provided evidence that ADK activity was dramatically

https://doi.org/10.1021/acsmaterialslett.3c00256
ACS Materials Lett. 2023, 5, 2028−2038

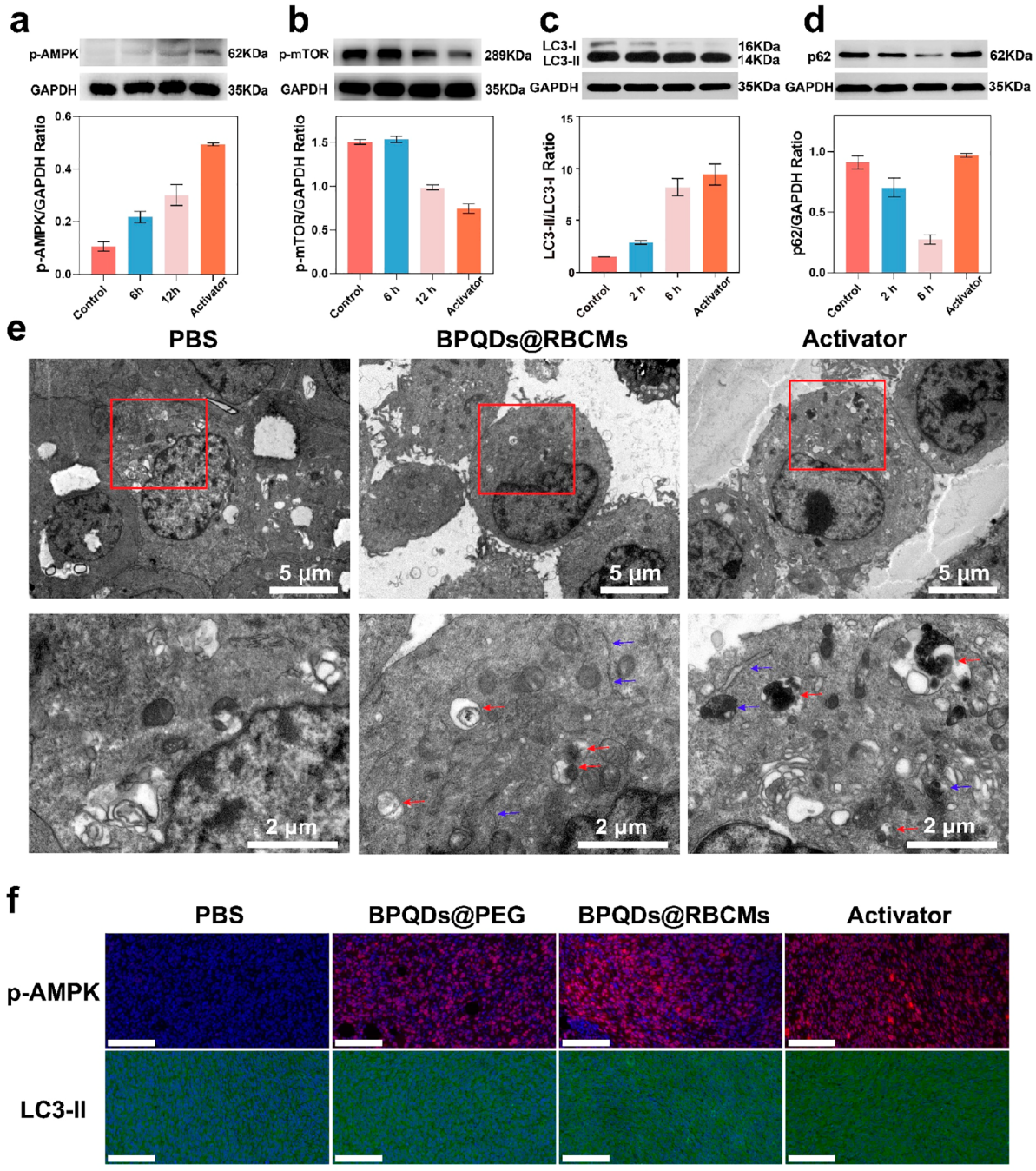

Figure 3. BPQDs@RBCMs trigger autophagy in cancer cells after promoting anabolism. (a−d) Western blot of p-AMPK (a), p-mTOR (b) after treatment with BPQDs@RBCMs for 6 and 12 h, LC3-II/LC3-I (c), and p62 (d) after treatment with BPQDs@RBCMs for 2 and 6 h, and the corresponding relative band intensity. Glyceraldehyde-3-phosphate dehydrogenase (GAPDH) expression level served as control. PBS and autophagy activator rapamycin were also treated as blank and positive control. Data are means ± SD (n = 3). (e) TEM images of 5637 cells treated with PBS, BPQDs@RBCMs and autophagy activator rapamycin for 24 h. Blue arrows indicate isolation membranes and autophagosomes, and red arrows indicate autolysosomes. (f) Fluorescence imaging of p-AMPK and autophagy protein LC3-II in tumor sections treated by PBS (the blank control), BPQDs@PEG (the negative control), BPQDs@RBCMs, and autophagy activator rapamycin (the positive control). Fluorescent-labeled p-AMPK and LC3-II in BPQDs@RBCMs and rapamycin-treated cells were much brighter than those in PBS and BPQDs@PEG-treated cells. The tumor model was established by subcutaneously injecting 5637 cells into the axilla of mice. Scale bar: 100 μm.

enhanced by BPQDs@RBCMs degradation and generated phosphate, leading to more AMP and ADP production and promotion of anabolism.

Next, the degradation behavior and ability of BPQDs@RBCMs to regulate the cellular energy levels were explored. We first determined whether intracellular ADK expression was affected by BPQDs@RBCMs. The intracellular localization of ADK in MC3T3 normal cells or 5637 cancer cells was monitored using fluorescent conjugated antibodies after BPQDs@RBCMs treatment. The results suggest that ADK expressions were not affected by BPQDs@RBCMs treatment (Figures 2c and S7). To investigate the degradation behavior

https://doi.org/10.1021/acsmaterialslett.3c00256
ACS Materials Lett. 2023, 5, 2028−2038

of BPQDs@RBCMs in normal and cancer cells, we examined the total area of three characteristic Raman peaks. The results show relatively moderate biodegradation of BPQDs@RBCMs in normal cells, whereas accelerated biodegradation of BPQDs@RBCMs in a time-dependent manner was observed in cancer cells due to acidity and strong intracellular oxidative stress (Figure 2d), implying the selective degradation of BPQDs@RBCMs in cancer cells. The rise in the ADP/ATP and AMP/ATP ratios signifies falling energy levels.[14,18] To identify whether the selective degradation leads to falling energy levels, the change in AMP/ATP and ADP/ATP ratios at predetermined time intervals was measured by high performance liquid chromatography (HPLC) (Figure 2e and 2f). In cancer cells, the AMP/ATP and ADP/ATP ratios increased remarkably with extending incubation time of BPQDs@RBCMs, while the ratios in normal cells did not change significantly.

To confirm the effective anabolism promotion of BPQDs@RBCMs in other cancer cells, the biodegradation of BPQDs@RBCMs and the resultant changes in energy levels were also determined in SCC-7 cell lines. With the extended incubation time, the Raman intensity of the three characteristic peaks of BPQDs in SCC-7 cells dropped remarkably, while that in MC3T3 cells was less affected (Figure S8). Further, the intracellular AMP/ATP and ADP/ATP ratios were detected by HPLC (Figure S9). Similar to the results in 5637 cell lines, the BPQDs@RBCMs treatment of 24 h obviously decreases the energy levels of SCC-7 cells, whereas the energy levels are relative stable in MC3T3 cells, demonstrating the effective anabolism activation in SCC-7 cells.

Altogether, the selective degradation of BPQDs@RBCMs in the tumor microenvironment promotes anabolism and lowers the energy levels via ADK-catalyzed reaction (Figure 2g). These processes have immense potential in tumor-selective autophagy activation.

AMPK is the cellular energy sensor.[1,18] Once activated by falling energy levels, phosphorylated AMPK directly triggers autophagy and further inhibits the suppressive effect of mTOR on autophagy.[14,19,36,37] Next, we identified whether BPQDs@RBCMs-promoted anabolism leads to autophagy through the AMPK pathways. Western blot analysis was conducted to assess the abundance of phosphorylated AMPK (p-AMPK) and phosphorylated mTOR (p-mTOR) in 5637 cells after BPQDs@RBCMs treatment. Western blot analysis showed an increased level of p-AMPK and a reduced level of p-mTOR in BPQDs@RBCMs-treated cells after 12 h compared to phosphate buffered saline (PBS) control group (Figure 3a and 3b). In 3D-cultured 5637 cells, BPQDs@RBCMs treatment for 12 h also obviously upregulates p-AMPK in comparison with the PBS control group (Figure S10), demonstrating that BPQDs@RBCMs treatment caused significant activation of AMPK and inhibition of mTOR activity. In the following, we addressed whether BPQDs@RBCMs treatment induces autophagy upon AMPK phosphorylation. Previous studies have identified that LC3-I is covalently conjugated to phosphatidylethanolamine to form autophagosome-membrane-bound LC3-II,[38,39] and sequestrosome-1 (p62) is also degraded in the autolysosome during autophagy.[40] Thus, the ratio of LC3-II/LC3-I and the levels of p62 are widely used to monitor autophagic activity. The conversion of LC3-I to LC3-II and cellular levels of p62 in BPQDs@RBCMs-treated 5637 cells were detected using Western blot analysis. The results reveal that BPQDs@RBCMs treatment resulted in a significant increase of cellular LC3-II/LC3-I ratios (Figure 3c) and a decrease in p62 protein levels (Figure 3d). The above results demonstrate that BPQDs@RBCMs, by promoting anabolism, successfully activate autophagy in cancer cells through AMPK phosphorylation and mTOR inhibition.

Autophagic structures were also observed in BPQDs@RBCMs-treated cells to confirm autophagy induction. During autophagy, intracellular contents such as organelles are engulfed by isolation membrane to form double-membrane autophagosomes, autophagosomes then fuse with lysosomes to form single-membrane autolysosomes.[38,41,42] In this process, autophagosome and autolysosome formation marks the occurrence of autophagy in the cell.[43] TEM was used to further detect the formation of isolation membranes, autophagosomes, and autolysosomes in 5637 cells treated with BPQDs@RBCMs. Clear isolation membranes and autophagosomes (blue arrows) that wrap and engulf portions of cytoplasm and organelles, and autolysosomes (red arrows), where sequestered organelles were degraded, were observed in cells treated with BPQDs@RBCMs or autophagy activator rapamycin (the positive control inhibiting mTOR activity and activating autophagy), whereas almost no autophagosome or autolysosome was observed in the PBS control (Figure 3e). These results also suggest that BPQDs@RBCMs exposure leads to obvious autophagy in cancer cells.

To investigate whether the BPQDs@RBCMs treatment could switch on AMPK pathways to trigger autophagy in other tumor models, Western blot analysis for p-AMPK, p-mTOR and LC3 expressions was also conducted in SCC-7 cells (Figure S11). Similarly, the levels of p-AMPK and p-mTOR increased and decreased, respectively, after BPQDs@RBCMs treatment, together with the increase in LC3-II levels, demonstrating the AMPK activation and autophagy induction in SCC-7 cells. Furthermore, TEM was used to observe the autophagic structures in SCC-7 cells after adding BPQDs@RBCMs (Figure S12). Compared to the PBS-treated group, BPQDs@RBCMs and autophagy activator rapamycin increased the number of autophagosomes or autolysosomes in SCC-7 cells. Together, these results suggest that BPQDs@RBCMs can activate AMPK and inhibit mTOR activity to induce autophagy in multiple cancer cells.

Moreover, to fully elucidate the influence of increased anabolism on the AMPK pathway and autophagy, levels of p-AMPK and LC3-II were evaluated *in vivo* using 5637 tumor-bearing mice after BPQDs@RBCMs treatment. The mice were randomly divided into four groups and treated with PBS (the blank control), autophagy activator rapamycin (the positive control), BPQDs@PEG (the negative control, the degradation of BPQDs will get slower after polyethylene glycol (PEG) modification) and BPQDs@RBCMs. At 24 h after injection, we performed immunohistochemical analysis using antibodies against p-AMPK and LC3-II in tumor sections, and observed the expressions of p-AMPK and LC3-II by confocal laser scanning fluorescence imaging. As shown in Figure 3f, BPQDs@RBCMs treatment results in increased levels of p-AMPK and LC3-II, confirming the BPQDs@RBCMs-induced increase in autophagic activity. Overall, these results pointed out that BPQDs@RBCMs can obviously activate autophagy via AMPK phosphorylation in response to enhanced anabolism.

Autophagy activation can suppress tumor growth in the tumor-initiation stage by maintaining intracellular energy

https://doi.org/10.1021/acsmaterialslett.3c00256
ACS Materials Lett. 2023, 5, 2028−2038

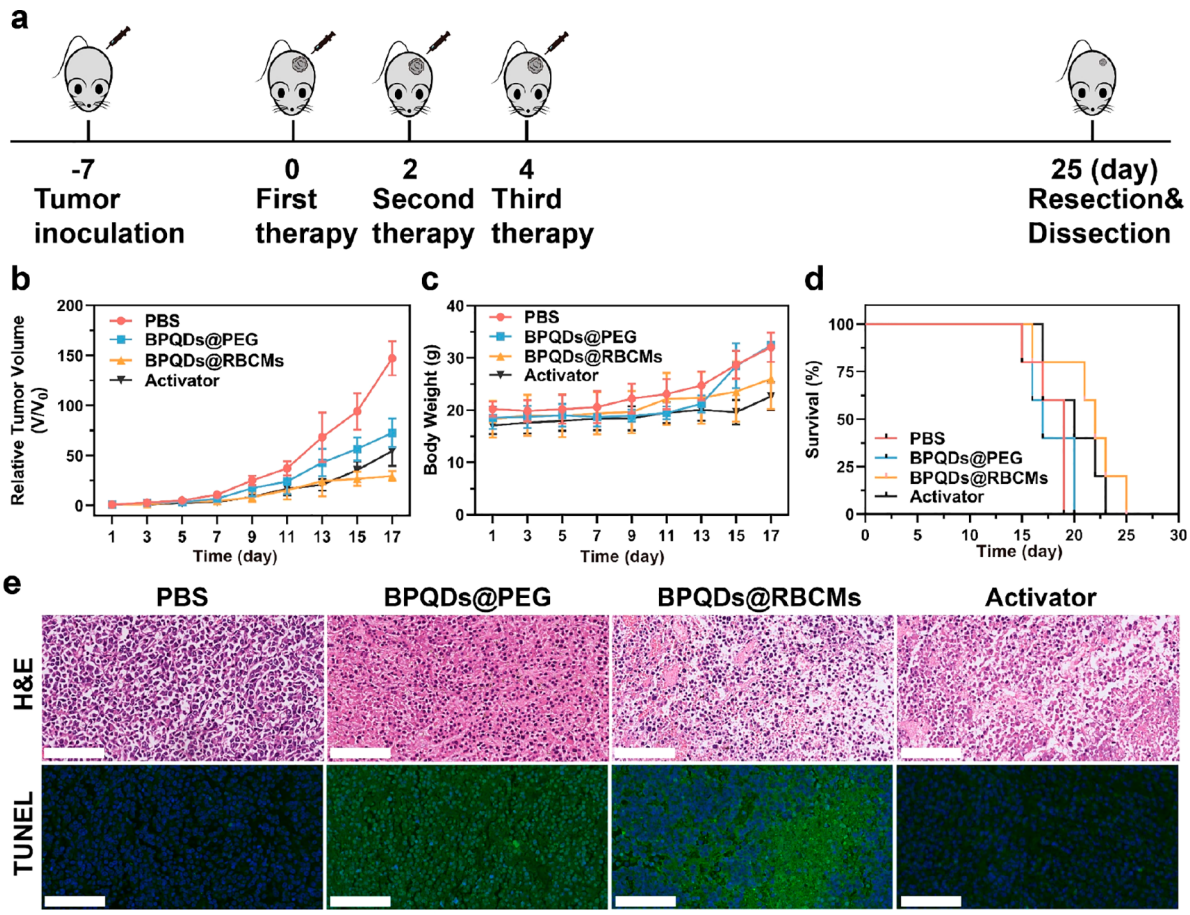

Figure 4. Tumor suppression effect of BPQDs@RBCMs. (a) Experimental design to evaluate the tumor suppression effect of BPQDs@RBCMs. Mice were inoculated with 5637 bladder cancer cells in the right axillary area. When the tumor diameter reached 100 cm^3, the mice were randomly divided into four groups that were treated with PBS, rapamycin, and BPQDs@PEG and BPQDs@RBCMs, respectively. All the mice were injected intravenously with above solutions every 2 days for a total of 3 times. Then the tumor growth and the survival time of mice were monitored up to 25 days, at which point the last mouse was killed. (b) Tumor growth curves of tumor-bearing mice with different treatment methods. The tumor volume was normalized to the initial size before treatment. The tumor volume ratio (V/V_0) of the PBS-treated group increased by four times compared with the BPQDs@RBCMs-treated group. Data are means ± SD (n = 5). (c) Body weight of mice during treatment. Data are means ± SD (n = 5). (d) The survival curves of tumor-bearing mice receiving different treatments. The mice treated with BPQDs@RBCMs had been longest-term survivors and had a life span of 25 days. Data are means ± SD (n = 5). (e) H&E and TUNEL staining of mice tumor tissues with different treatments. Scale bar: 50 μm.

homeostasis.[44] To identify whether BPQDs@RBCMs treatment and autophagy activation lead to tumor suppression, the influences of BPQDs@RBCMs on tumors were evaluated using tumor-bearing mice xenografted with 5637 cells as models. We first investigated the *in vivo* metabolic behavior of BPQDs@RBCMs. Near-infrared dye Cy5.5-labeled BPQDs@RBCMs with bright fluorescence at about 710 nm were synthesized (Figure S13), thereby enabling the monitoring of BPQDs@RBCMs biodistribution in mice.[45] After being intravenously injected with the Cy5.5-labeled BPQDs@RBCMs, the pharmacokinetics profile and biodistribution of BPQDs@RBCMs were obtained by fluorescence imaging (Figures S14 and S15). BPQDs@RBCMs continuously accumulated at the tumor site for up to 24 h. The results suggest the good retention of the BPQDs@RBCMs in the body, indicating the evasion of the immune system and extended blood circulation half-life.

We then examined the suppressive effects of BPQDs@RBCMs on tumor growth after promoting anabolism and activating autophagy. The mice were randomly divided into four groups and treated with PBS (the blank control), autophagy activator rapamycin (the positive control), BPQDs@PEG (the negative control), and BPQDs@RBCMs. The treatment was conducted by intratumoral injection three times for every 2 days in the first 6 days, the volume and mass of all tumors were continuously monitored until mice were killed, then tumor sections were collected and the histological analyses were performed (Figure 4a). Tumor growth curves plotted in Figure 4b show that BPQDs@RBCMs and rapamycin treatment inhibited tumor growth effectively. No meaningful difference of body weight can be observed during the whole-treatment period from all of the groups (Figure 4c). The life spans of all of the groups were further investigated (Figure 4d). BPQDs@RBCMs and rapamycin-treated mice had a longer survival than those treated with PBS or BPQDs@PEG, demonstrating that autophagy activation prolonged the survival of mice obviously. Finally, the anticancer efficiency of BPQDs@RBCMs was checked by immunohistochemistry including hematoxylin and eosin (H&E) staining and terminal deoxynucleotidyl transferase-mediated deoxyuridine triphosphate nick end-labeling (TUNEL) assay. The images of TUNEL stained tumor slices show a significantly higher level

https://doi.org/10.1021/acsmaterialslett.3c00256
ACS Materials Lett. 2023, 5, 2028−2038

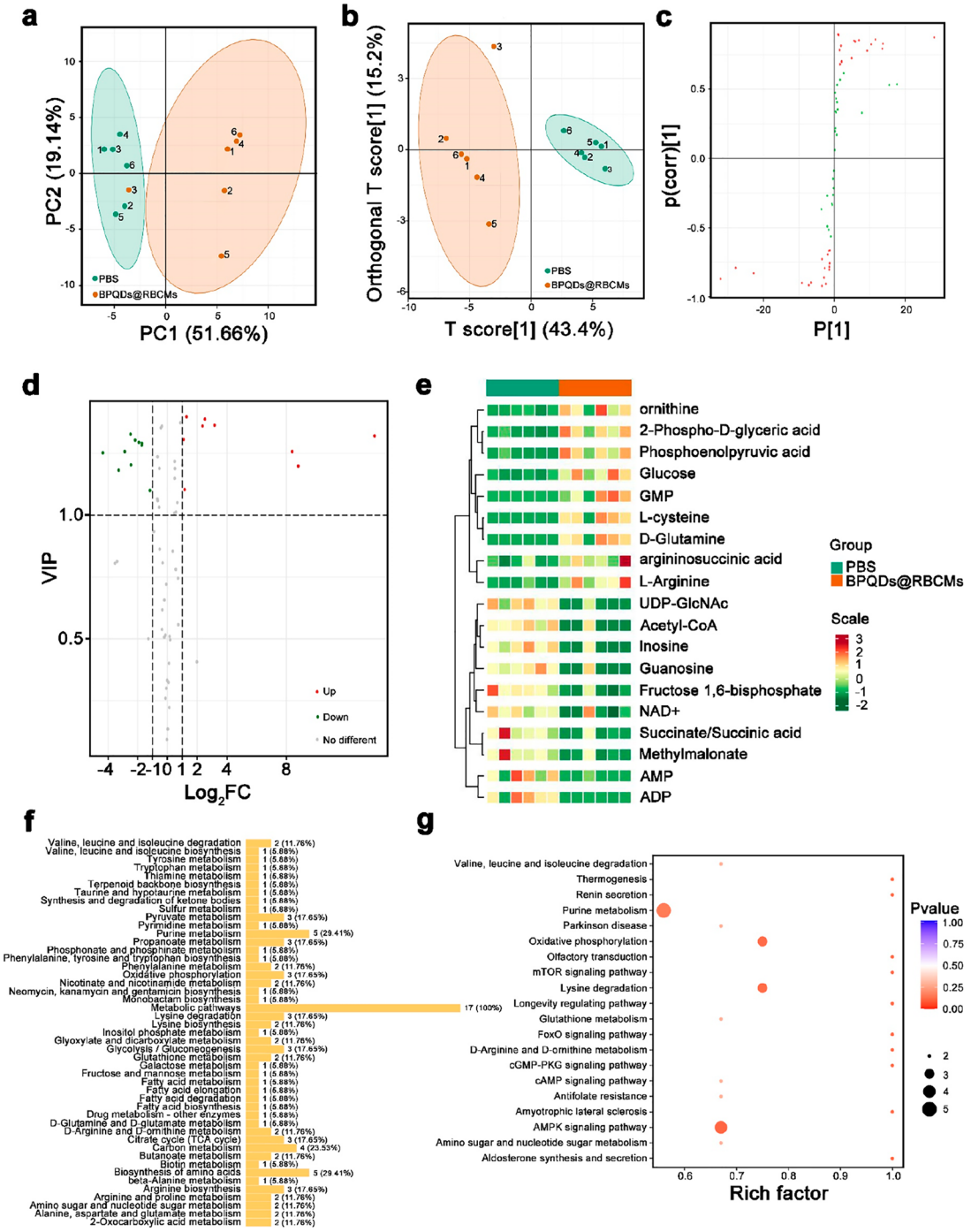

Figure 5. Metabolic analysis of tumor tissues treated by BPQDs@RBCMs and PBS. (a) PCA diagram of metabolites after PBS or BPQDs@RBCMs treatment in tumor. Significantly altered metabolites were identified between PBS and BPQDs@RBCMs-treated group. (b) OPLS-DA score chart of metabolites after PBS or BPQDs@RBCMs treatment in tumor. OPLS-DA further aided in differentiating the two groups. (c) S-plot of OPLS-DA. The variable importance in projection (VIP) is the weighted sum of the squares of the OPLS-DA analysis. Red dots indicate that the VIP scores of these metabolites are greater than or equal to 1, and VIP scores of green dots are less than 1. Metabolites that meet the condition of VIP > 1 are the most implicated in the differences between the two groups. (d) Volcano plot of differential metabolites. Green dots represent downregulated metabolites, red dots represent upregulated metabolites, and gray dots represent metabolites with insignificant differences. A total of 19 differential metabolites were identified, with 9 upregulated metabolites and 10 downregulated metabolites. (e) Hierarchically clustered heatmaps of differential metabolites after PBS or BPQDs@RBCMs treatment in tumor. The color from green to red indicates that the relative content of metabolites increases successively. (f) Classification of differential metabolites according to the KEGG database. The differential metabolites were assigned to the metabolic pathways stored in the KEGG database to gain insights into the changes in metabolite profiles. (g) Pathway enrichment analysis of differential metabolites after PBS or BPQDs@RBCMs treatment in tumor. The abscissa is the Rich factor. The greater the Rich factor, the greater the enrichment degree will be. The color change from red to blue indicates that the P value increases successively. Pathways are shown as dots, and the dot size was determined by the number of differential metabolites in each pathway, with a bigger dot corresponding to more metabolites enriched in this pathway.

https://doi.org/10.1021/acsmaterialslett.3c00256
ACS Materials Lett. 2023, 5, 2028−2038

of cell death in the group treated with BPQDs@RBCMs (Figure 4e). Taken together, these results indicate that BPQDs@RBCMs can inhibit tumor growth after anabolism is promoted and activating autophagy.

Autophagy activation has a crucial regulatory role in energy metabolism and, thereby, might normalize the tumor metabolism. To confirm the regulatory role of BPQDs@RBCMs-induced autophagy in tumor metabolism, the changes in the representative 61 metabolites were determined in the tumor tissues of mice treated with PBS or BPQDs@RBCMs. To identify whether the tumor metabolome of the BPQDs@RBCMs-treated group differs from that of the PBS-treated group, principal component analysis (PCA) and orthogonal partial least-squares discriminant analysis (OPLS-DA) were performed to evaluate the differences of metabolites between the two groups. As seen in Figure 5a and 5b, a clear separation between the two groups suggests that the metabolome was quite different after BPQDs@RBCMs-induced autophagy.

Next, we sought to identify the metabolites that were significantly different in the two groups after autophagy activation. Preliminary metabolite identification can be achieved by finding metabolites of variable importance in projection (VIP) scores >1.[46,47] In the S-plot of the OPLS-DA model (Figure 5c), 33 metabolites with a VIP score >1 were identified, indicating a significant difference of these metabolites between the two groups. Volcano plots and violin plots further provided a quick look at the differences in the two groups for a more accurate comparison of metabolites (Figures 5d and S16), and 19 significantly altered metabolites were identified. To intuitively show the differences of the 19 metabolites, we applied heatmap with hierarchical clustering for the two groups (Figure 5e). The data demonstrated that BPQDs@RBCMs treatment induced significant changes in the levels of metabolites to restore the energy balance (Figure S17). Evidenced by the AMP, ADP and NAD^+ consumption in tumor, autophagy activation causes the energy status to be displaced toward ATP production to remain in balance with BPQDs@RBCMs-promoted anabolism.[20]

Finally, we investigated how BPQDs@RBCMs-induced autophagy regulates tumor metabolism. Mapping the altered metabolites to Kyoto Encyclopedia of Genes and Genomes (KEGG) pathways can help identify the alterations in various metabolic processes.[48] Figure 5f displays the classification of 19 differential metabolites into metabolic pathways as defined by the KEGG database. We identified that all the differential metabolites are associated with the regulations of the metabolic pathway. The pathway enrichment analysis of metabolites was next performed according to the classification of differential metabolites (Figure 5g). These results indicate that autophagy triggered by BPQDs@RBCMs involved the variations of several key metabolic pathways such as the AMPK signaling pathway, purine metabolism, and oxidative phosphorylation. These alterations imply reprogrammed anabolism and catabolism by BPQDs@RBCMs degradation and ensuing autophagy activation. Overall, these data suggested that BPQDs@RBCMs treatment considerably altered the metabolite profile of the tumor, demonstrating the successful regulation of tumor metabolism by autophagy.

In summary, we demonstrate the utility of BPQDs@RBCMs for promoting anabolism in cancer cells and delineate a new strategy to selectively trigger autophagy and to reprogram tumor metabolism. *In vitro* studies confirm that the selective biodegradation of BPQDs@RBCMs releasing phosphate in the tumor microenvironment activated the ADK-catalyzed reaction, followed by the tumor-selective promotion of anabolism and falling energy levels. Then, we found that BPQDs@RBCMs treatment caused the AMPK phosphorylation and inhibition of mTOR phosphorylation in cancer cells. Also, autophagosome and autolysosome formation was observed in cancer cells upon BPQDs@RBCMs treatment. The *in vivo* results further demonstrate the good retention of the BPQDs@RBCMs in the tumor, and the BPQDs@RBCMs treatment effectively reduced the overall tumor burden and extended the survival in tumor-bearing mice. Metabolic analysis indicated that BPQDs@RBCMs-induced autophagy resulted in significant changes in metabolites. This study not only demonstrates the role of anabolism in autophagy induction but also underlines the potential utility of selective autophagy induction as a new cancer treatment modality.

■ ASSOCIATED CONTENT

Supporting Information

The Supporting Information is available free of charge at https://pubs.acs.org/doi/10.1021/acsmaterialslett.3c00256.

Materials and methods, the characterization of BPQDs, RBCMs, and BPQDs@RBCMs, the degradation of BPQDs@RBCMs monitored by UV−vis spectrum, the BPQDs@RBCMs-induced autophagy in SCC-7 cells and 3D-cultured 5637 cells, the enzymatic kinetic of ADK, the intracellular ADK content, the blood circulation and biodistribution of BPQDs@RBCMs, and the violin plot and fold changes of 19 differential metabolites (PDF)

■ AUTHOR INFORMATION

Corresponding Authors

Jie Tan − *Molecular Science and Biomedicine Laboratory (MBL), State Key Laboratory of Chemo/Biosensing and Chemometrics, College of Chemistry and Chemical Engineering, Hunan University, Changsha 410082, China;* orcid.org/0000-0002-0909-2904; Email: tanjie0416@hnu.edu.cn

Quan Yuan − *Molecular Science and Biomedicine Laboratory (MBL), State Key Laboratory of Chemo/Biosensing and Chemometrics, College of Chemistry and Chemical Engineering, Hunan University, Changsha 410082, China;* orcid.org/0000-0002-3085-431X; Email: yuanquan@whu.edu.cn

Authors

Yiqi Li − *Molecular Science and Biomedicine Laboratory (MBL), State Key Laboratory of Chemo/Biosensing and Chemometrics, College of Chemistry and Chemical Engineering, Hunan University, Changsha 410082, China*

Qilong Fang − *Molecular Science and Biomedicine Laboratory (MBL), State Key Laboratory of Chemo/Biosensing and Chemometrics, College of Chemistry and Chemical Engineering, Hunan University, Changsha 410082, China*

Jiang-Yi-Hui Sheng − *Molecular Science and Biomedicine Laboratory (MBL), State Key Laboratory of Chemo/Biosensing and Chemometrics, College of Chemistry and Chemical Engineering, Hunan University, Changsha 410082, China;* orcid.org/0000-0001-7091-3460

Xiaodong Hu − *Molecular Science and Biomedicine Laboratory (MBL), State Key Laboratory of Chemo/*

Biosensing and Chemometrics, College of Chemistry and Chemical Engineering, Hunan University, Changsha 410082, China

Yanbing Yang − *College of Chemistry and Molecular Sciences, Wuhan University, Wuhan 430072, China*

Yun Zhang − *State Key Laboratory of Structural Chemistry, Fujian Institute of Research on the Structure of Matter, Chinese Academy of Sciences, Fuzhou 350002, China;* orcid.org/0000-0001-6288-4671

Long Chen − *Department of Computer and Information Science, Faculty of Science and Technology, University of Macau, Taipa 999078, Macau SAR, China*

Weihong Tan − *Molecular Science and Biomedicine Laboratory (MBL), State Key Laboratory of Chemo/Biosensing and Chemometrics, College of Chemistry and Chemical Engineering, Hunan University, Changsha 410082, China;* orcid.org/0000-0002-8066-1524

Complete contact information is available at: https://pubs.acs.org/10.1021/acsmaterialslett.3c00256

Author Contributions

‡Y.L., Q.F., J.S., and X.H. contributed equally to this work.

Notes

The authors declare no competing financial interest.

■ ACKNOWLEDGMENTS

This work was supported by Natural Science Foundation of Hunan Province (2022JJ20005), National Natural Science Foundation of China (22174038, 21925401, 52221001), the New Cornerstone Science Foundation through the XPLORER PRIZE, and the funding from the National Key R&D Program of China (2017YFA0208000).

■ REFERENCES

(1) Herzig, S.; Shaw, R. J. AMPK: guardian of metabolism and mitochondrial homeostasis. *Nat. Rev. Mol. Cell Biol.* **2018**, *19*, 121−135.

(2) Steinberg, G. R.; Hardie, D. G. New insights into activation and function of the AMPK. *Nat. Rev. Mol. Cell Biol.* **2023**, *24*, 255−272.

(3) Farrow, J. M.; Yang, J. C.; Evans, C. P. Autophagy as a modulator and target in prostate cancer. *Nat. Rev. Urol.* **2014**, *11*, 508−516.

(4) Rabinowitz, J. D.; White, E. Autophagy and metabolism. *Science* **2010**, *330*, 1344−1348.

(5) Li, J. J.; Hartono, D.; Ong, C.-N.; Bay, B.-H.; Yung, L.-Y. L. Autophagy and oxidative stress associated with gold nanoparticles. *Biomaterials* **2010**, *31*, 5996−6003.

(6) Xia, H.; Green, D. R.; Zou, W. Autophagy in tumour immunity and therapy. *Nat. Rev. Cancer* **2021**, *21*, 281−297.

(7) Janku, F.; McConkey, D. J.; Hong, D. S.; Kurzrock, R. Autophagy as a target for anticancer therapy. *Nat. Rev. Clin. Oncol.* **2011**, *8*, 528−539.

(8) Rubinsztein, D. C.; Codogno, P.; Levine, B. Autophagy modulation as a potential therapeutic target for diverse diseases. *Nat. Rev. Drug Discovery* **2012**, *11*, 709−730.

(9) Levy, J. M. M.; Towers, C. G.; Thorburn, A. Targeting autophagy in cancer. *Nat. Rev. Cancer* **2017**, *17*, 528−542.

(10) Kondo, Y.; Kanzawa, T.; Sawaya, R.; Kondo, S. The role of autophagy in cancer development and response to therapy. *Nat. Rev. Cancer* **2005**, *5*, 726−734.

(11) Galluzzi, L.; Bravo-San Pedro, J. M.; Levine, B.; Green, D. R.; Kroemer, G. Pharmacological modulation of autophagy: therapeutic potential and persisting obstacles. *Nat. Rev. Drug Discovery* **2017**, *16*, 487−511.

(12) Whitmarsh-Everiss, T.; Laraia, L. Small molecule probes for targeting autophagy. *Nat. Chem. Biol.* **2021**, *17*, 653−664.

(13) Rubinsztein, D. C.; Gestwicki, J. E.; Murphy, L. O.; Klionsky, D. J. Potential therapeutic applications of autophagy. *Nat. Rev. Drug Discovery* **2007**, *6*, 304−312.

(14) Hardie, D. G.; Ross, F. A.; Hawley, S. A. AMPK: a nutrient and energy sensor that maintains energy homeostasis. *Nat. Rev. Mol. Cell Biol.* **2012**, *13*, 251−262.

(15) Frederich, M.; O'Rourke, M. R.; Furey, N. B.; Jost, J. A. AMP-activated protein kinase (AMPK) in the rock crab, cancer irroratus: an early indicator of temperature stress. *J. Exp. Biol.* **2009**, *212*, 722−730.

(16) Gomes, L. C.; Benedetto, G. D.; Scorrano, L. During autophagy mitochondria elongate, are spared from degradation and sustain cell viability. *Nat. Cell Biol.* **2011**, *13*, 589−598.

(17) Dikic, I.; Elazar, Z. Mechanism and medical implications of mammalian autophagy. *Nat. Rev. Mol. Cell Biol.* **2018**, *19*, 349−364.

(18) Hardie, D. G. AMP-activated/SNF1 protein kinases: conserved guardians of cellular energy. *Nat. Rev. Mol. Cell Biol.* **2007**, *8*, 774−785.

(19) Zhang, C.-S.; Lin, S.-C. AMPK promotes autophagy by facilitating mitochondrial fission. *Cell Metab.* **2016**, *23*, 399−401.

(20) Kaur, J.; Debnath, J. Autophagy at the crossroads of catabolism and anabolism. *Nat. Rev. Mol. Cell Biol.* **2015**, *16*, 461−472.

(21) Park, J.; Gupta, R. S. Adenosine kinase and ribokinase - the RK family of proteins. *Cell. Mol. Life Sci.* **2008**, *65*, 2875−2896.

(22) Bi, Q.-C.; Luo, R.-G.; Li, Y.-S.; Zhao, J.; Fu, X.; Chen, H.; Lv, Y.-F.; Liu, Z.-X.; Liang, Q.-R.; Tang, Q. Low inorganic phosphate stress inhibits liver cancer progression: from *in vivo* to *in vitro*. *Adv. Therap.* **2022**, *5*, 2100224.

(23) Zhou, W.; Pan, T.; Cui, H.; Zhao, Z.; Chu, P. K.; Yu, X.-F. Black phosphorus: bioactive nanomaterials with inherent and selective chemotherapeutic effects. *Angew. Chem., Int. Ed.* **2019**, *58*, 769−774.

(24) Pei, Q.; Hu, X.; Zheng, X.; Liu, S.; Li, Y.; Jing, X.; Xie, Z. Light-activatable red blood cell membrane-camouflaged dimeric prodrug nanoparticles for synergistic photodynamic/chemotherapy. *ACS Nano* **2018**, *12*, 1630−1641.

(25) Gao, W.; Hu, C.-M. J.; Fang, R. H.; Luk, B. T.; Su, J.; Zhang, L. Surface functionalization of gold nanoparticles with red blood cell membranes. *Adv. Mater.* **2013**, *25*, 3549−3553.

(26) Zhou, W.; Cui, H.; Ying, L.; Yu, X.-F. Enhanced cytosolic delivery and release of CRISPR/Cas9 by black phosphorus nanosheets for genome editing. *Angew. Chem., Int. Ed.* **2018**, *57*, 10268−10272.

(27) Liu, W.; Dong, A.; Wang, B.; Zhang, H. Current advances in black phosphorus-based drug delivery systems for cancer therapy. *Adv. Sci.* **2021**, *8*, 2003033.

(28) Yamada, Y.; Goto, H.; Ogasawara, N. Purification and properties of adenosine kinase from rat brain. *Biochim. Biophys. Acta-Enzym.* **1980**, *616*, 199−207.

(29) Palella, T. D.; Andres, C. M.; Fox, I. H. Human placental adenosine kinase. Kinetic mechanism and inhibition. *J. Biol. Chem.* **1980**, *255*, 5264−5269.

(30) de Jong, J. W.; Keijzer, E.; Huizer, T.; Schoutsen, B. Ischemic nucleotide breakdown increases during cardiac development due to drop in adenosine anabolism/catabolism ratio. *J. Mol. Cell. Cardiol.* **1990**, *22*, 1065−1070.

(31) Smee, D. F.; Matthews, T. R. Metabolism of ribavirin in respiratory syncytial virus-infected and uninfected cells. *Antimicrob. Agents Chemother.* **1986**, *30*, 117−121.

(32) Maj, M.; Singh, B.; Gupta, R. S. The influence of inorganic phosphate on the activity of adenosine kinase. *Biochim. Biophys. Acta-Protein Struct. Mol. Enzym.* **2000**, *1476*, 33−42.

(33) Park, J.; Singh, B.; Maj, M. C.; Gupta, R. S. Phosphorylated derivatives that activate or inhibit mammalian adenosine kinase provide insights into the role of pentavalent ions in AK catalysis. *Protein J.* **2004**, *23*, 167−177.

(34) Boison, D.; Jarvis, M. F. Adenosine kinase: a key regulator of purinergic physiology. *Biochem. Pharmacol.* **2021**, *187*, 114321.

(35) Boison, D. Adenosine Kinase: exploitation for therapeutic gain. *Pharmacol. Rev.* **2013**, *65*, 906.

(36) Kim, Y. C.; Guan, K.-L. mTOR: a pharmacologic target for autophagy regulation. *J. Clin. Invest.* **2015**, *125*, 25−32.
(37) Hawley, S. A.; Ross, F. A.; Chevtzoff, C.; Green, K. A.; Evans, A.; Fogarty, S.; Towler, M. C.; Brown, L. J.; Ogunbayo, O. A.; Evans, A. M.; Hardie, D. G. Use of cells expressing γ subunit variants to identify diverse mechanisms of AMPK activation. *Cell Metab.* **2010**, *11*, 554−565.
(38) Ma, X.; Wu, Y.; Jin, S.; Tian, Y.; Zhang, X.; Zhao, Y.; Yu, L.; Liang, X.-J. Gold nanoparticles induce autophagosome accumulation through size-dependent nanoparticle uptake and lysosome impairment. *ACS Nano* **2011**, *5*, 8629−8639.
(39) Zhu, M.; Du, L.; Zhao, R.; Wang, H. Y.; Zhao, Y.; Nie, G.; Wang, R.-F. Cell-penetrating nanoparticles activate the inflammasome to enhance antibody production by targeting microtubule-associated protein 1-light chain 3 for degradation. *ACS Nano* **2020**, *14*, 3703−3717.
(40) Ueno, T.; Komatsu, M. Monitoring autophagy flux and activity: principles and applications. *BioEssays* **2020**, *42*, 2000122.
(41) Cabezudo, S.; Sanz-Flores, M.; Caballero, A.; Tasset, I.; Rebollo, E.; Diaz, A.; Aragay, A. M.; Cuervo, A. M.; Mayor, F.; Ribas, C. Gαq activation modulates autophagy by promoting mTORC1 signaling. *Nat. Commun.* **2021**, *12*, 4540.
(42) Li, X.; He, S.; Ma, B. Autophagy and autophagy-related proteins in cancer. *Mol. Cancer* **2020**, *19*, 12.
(43) Cui, W.; Yang, X.; Chen, X.; Xiao, D.; Zhu, J.; Zhang, M.; Qin, X.; Ma, X.; Lin, Y. Treating LRRK2-related parkinson's disease by inhibiting the mTOR signaling pathway to restore autophagy. *Adv. Funct. Mater.* **2021**, *31*, 2105152.
(44) White, E.; Karp, C.; Strohecker, A. M.; Guo, Y.; Mathew, R. Role of autophagy in suppression of inflammation and cancer. *Curr. Opin. Cell Biol.* **2010**, *22*, 212−217.
(45) Shao, J.; Xie, H.; Huang, H.; Li, Z.; Sun, Z.; Xu, Y.; Xiao, Q.; Yu, X.-F.; Zhao, Y.; Zhang, H.; Wang, H.; Chu, P. K. Biodegradable black phosphorus-based nanospheres for *in vivo* photothermal cancer therapy. *Nat. Commun.* **2016**, *7*, 12967.
(46) Yan, X.; Chen, S.; Pan, Z.; Zhao, W.; Rui, Y.; Zhao, L. AgNPs-triggered seed metabolic and transcriptional reprogramming enhanced rice salt tolerance and blast resistance. *ACS Nano* **2023**, *17*, 492−504.
(47) Diémé, B.; Mavel, S.; Blasco, H.; Tripi, G.; Bonnet-Brilhault, F.; Malvy, J.; Bocca, C.; Andres, C. R.; Nadal-Desbarats, L.; Emond, P. Metabolomics study of urine in autism spectrum disorders using a multiplatform analytical methodology. *J. Proteome Res.* **2015**, *14*, 5273−5282.
(48) Zhang, A.-H.; Sun, H.; Han, Y.; Yan, G.-L.; Yuan, Y.; Song, G.-C.; Yuan, X.-X.; Xie, N.; Wang, X.-J. Ultraperformance liquid chromatography-mass spectrometry based comprehensive metabolomics combined with pattern recognition and network analysis methods for characterization of metabolites and metabolic pathways from biological data sets. *Anal. Chem.* **2013**, *85*, 7606−7612.

https://doi.org/10.1021/acsmaterialslett.3c00256
ACS Materials Lett. 2023, 5, 2028−2038